Article

Photophysical Properties of Benzophenone-Based TADF Emitters in Relation to Their Molecular Structure

Ekin Esme Bas, Pelin Ulukan, Antonio Monari, Viktorya Aviyente,* and Saron Catak*

Read Online

ACCESS | 📊 Metrics & More | 📖 Article Recommendations | 🗂 Supporting Information

ABSTRACT: Thermally activated delayed fluorescence (TADF) materials are commonly used in various apparatus, including organic light-emitting device-based displays, as they remarkably improve the internal quantum efficiencies. Although there is a wide range of donor–acceptor-based compounds possessing TADF properties, in this computational study, we investigated TADF and some non-TADF chromophores, containing benzophenone or its structural derivatives as the acceptor core, together with various donor moieties. Following the computational modeling of the emitters, several excited state properties, such as the absorption spectra, singlet–triplet energy gaps (ΔE_{ST}), natural transition orbitals, and the topological Φ_S indices, have been computed. Along with the donor–acceptor torsion angles and spin-orbit coupling values, these descriptors

have been utilized to investigate potential TADF efficiency. Our study has shown that on the one hand, our photophysical/structural descriptors and computational methodologies predict the experimental results quite well, and on the other hand, our extensive benchmark can be useful to pinpoint the most promising functionals and descriptors for the study of benzophenone-based TADF emitters.
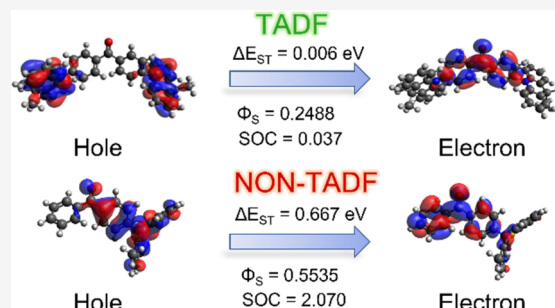
1. INTRODUCTION

Organic light-emitting diodes (OLEDs) have attracted widespread attention since the invention of the first organic electroluminescent device in 1987.[1] As compared to conventional LEDs and liquid crystal display systems, OLEDs do not require a backlight unit, as they are self-illuminating. Given this distinct feature, OLEDs offer several advantages, such as flexible device structures, decreased panel thickness, improved brightness, and reduced power consumption, rendering them most suitable for various devices.[2] Nevertheless, OLEDs also display serious efficiency drawbacks, which are grounded in the fundamental spin statistics rule (Figure 1) because the population of the nonemissive triplet state comprises 75% of the generated excitons in the device, hence leading to the loss of two thirds of the applied energy.[3] Phosphorescent organic light-emitting diodes (PhOLEDs), which contain heavy atoms, can improve the efficiencies of OLEDs with the help of enhanced intersystem crossing (ISC) and improved phosphorescence rates as a result of increased spin-orbit coupling (SOC).[4,5] However, heavy metals instigate environmental issues while significantly increasing the cost of the device, thus limiting the commercial availability of PhOLEDs.[6]

Thermally activated delayed fluorescence (TADF) materials, first proposed by Adachi et al. in 2011, represent a most suitable alternative to overcome spin statistics burdens and achieve high internal quantum efficiencies (IQEs) in OLED displays.[7] In TADF processes, the population of triplet excitons undergoes a slow reverse intersystem crossing (RISC), re-

populating the emissive first excited singlet state (S_1) and hence avoiding the inclusion of heavy metals. To assure efficiency, RISC or the upconversion of the triplet states [up-intersystem crossing (UISC)] require a small S_1-T_1 energy gap (ΔE_{ST}). UISC can be achieved by promoting the population of intramolecular charge-transfer (ICT) states and is usually, albeit not necessarily, correlated with a small gap between the highest occupied molecular orbital and lowest unoccupied molecular orbital. To achieve efficient ICT, the molecular architecture requires the presence of a donor (D) moiety bridged to an acceptor (A) (Figure 1). The D and A groups can be separated by using bulky substituents to increase steric effects and maintain orthogonal molecular structures, hence minimizing conjugation and delocalization, or alternatively by π-bridges.[8,9]

Benzophenone is a widely used building block in the design of OLED devices, in part due to its strong and efficient electron accepting and efficient ultraviolet (UV) absorbing abilities, as well as its high ISC efficiency.[10−13] Adachi and co-workers showed in 2014 that efficient deep blue TADF could
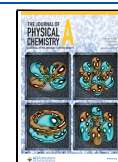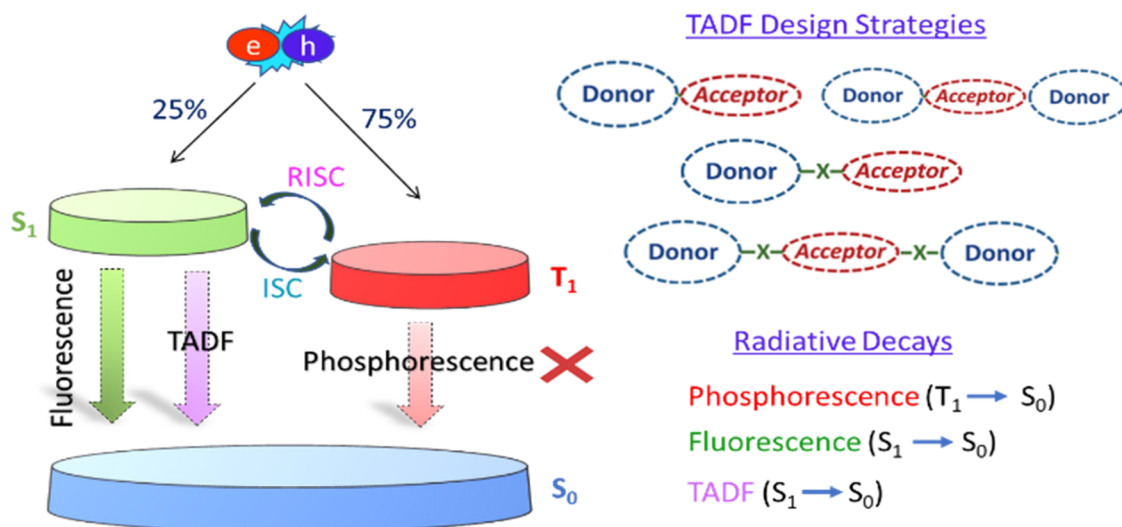
Figure 1. Schematic representation of ISC, RISC, TADF, and phosphorescence processes in a Jablonski diagram along with the possible design strategies for TADF emitters.

be achieved by using benzophenone-based D-A-D frameworks.[12] Thus far, many benzophenone-based TADF emitters possessing a small ΔE_{ST} have been reported to feature full-color delayed fluorescence emission, usually in a range from deep blue to green and with external quantum efficiencies up to 14.3%.[14] Benzophenone-based luminogens can also be used to induce aggregation-induced delayed fluorescence.[15,16]

Nonetheless, the rather floppy phenyl moieties of benzophenone itself may induce intramolecular rotations, which enhance nonradiative decay and lead to relatively low reverse ISC rates (k_{RISC}).[17] Hence, more compact and rigid benzophenone derivatives, such as anthraquinone,[18,19] xanthone,[20−23] dibenzothiophene-benzoyl[24,25] and phenylcarbazole-benzoyl,[26] are deemed more promising in terms of their TADF efficiencies. Figure 2 depicts the molecular structures of benzophenone derivatives commonly used in TADF materials, together with some of the most widely used D groups.

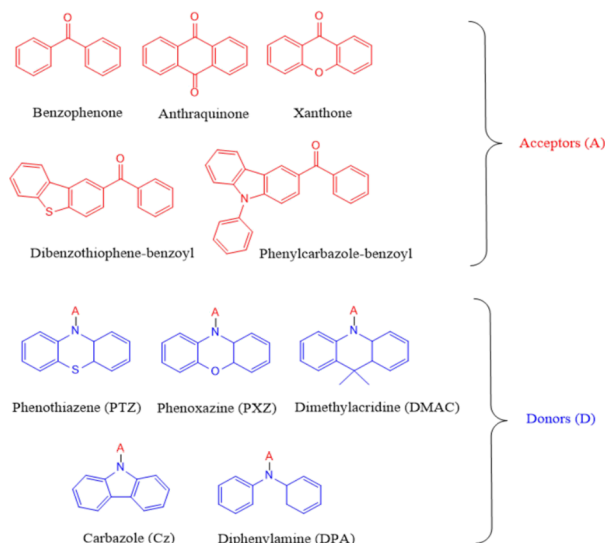We used molecular modeling to elucidate the relationship between the molecular structure and optimal photophysical properties that are essential for effective TADF emission. Various descriptors are used to define TADF properties, which include ΔE_{ST}, SOC, natural transition orbitals (NTOs), the topological Φ_S index quantifying the charge-transfer amount, and the torsion angles between D and A moieties.[27−33] The oscillator strength (f) is also a critical parameter to attain a reasonable radiative decay rate (k_r) from the S_1 state to the ground state. The oscillator strength is usually closer to 0 for orthogonal donor−acceptor compounds, where CT is prominent.[29] Negligible oscillator strengths represent a challenge in TADF emitters because it is essential to balance a small ΔE_{ST} and a sufficiently large k_r to reach high IQE in OLED devices.

In this study, a series of experimentally studied TADF emitters, employing benzophenone and its derivatives, have been investigated by quantum chemical calculations. Several non-TADF benzophenone chromophores have also been modeled for comparison. Absorption spectra of the selected compounds have been generated, including a sampling of the Franck−Condon region by Wigner distribution, to include dynamic effects. To determine the degree of charge separation in the excited state, NTOs and Φ_S indices have been computed, as well as the ΔE_{ST} values. NTO and ΔE_{ST} calculations have been performed on both the ground state (S_0) and the lowest triplet state (T_1) equilibrium geometries because geometrical reorganization can also play a role in photophysical processes. Furthermore, the SOCs between singlet and triplet excited states have been computed to better estimate RISC probability.

The mentioned descriptors have proven to be insightful in determining potential TADF efficiency, as well as shedding light on the correlation between molecular structure and TADF performance. Indeed, the investigation of the photophysical characteristics of both the excited and ground state geometries, and also the assessment of the DFT functionals for the excited state calculations of TADF emitters, may help provide a better understanding for the photophysical processes related to TADF at a molecular level.
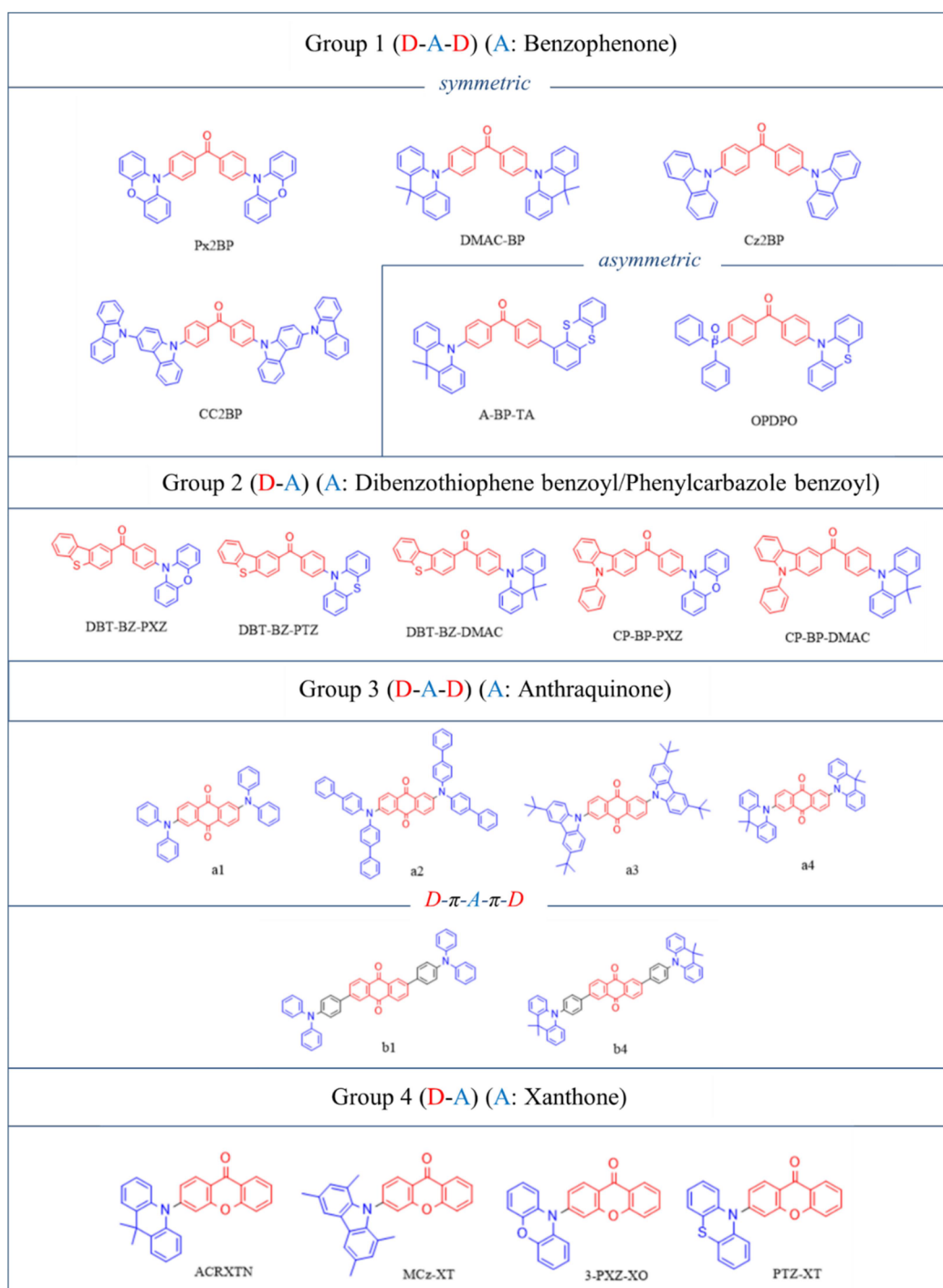

Figure 2. Electron-donating and -accepting moieties frequently used in the design of benzophenone-based TADF emitters.

Figure 3. Classification of TADF emitters modeled in this study.

2. METHODOLOGY

All ground state geometry optimizations have been performed using the Gaussian 16 program package,[34] and a comprehensive conformational search has been carried out. UV–vis absorption spectra and Boltzmann-weighted ΔE_{ST} calculations (Tables S1 and S2) showed that different conformations did not exhibit significant differences in their excitation energies and on the ordering of the excited states. Hence, T_1 geometry optimizations and related excited state calculations were carried out solely on the most stable conformer. The M06-2X functional[35] has been used together with the 6−31 + G(d,p) basis set for S_0 and T_1 geometry optimizations. This

choice is justified because M06-2X is well known to correctly reproduce medium-range interactions, electronic energies, and equilibrium geometries of compounds with aromatic ring systems.[35] However, a dispersion-corrected functional, B3LYP-D3, was also tested for the geometry optimization of rather larger compounds.[36] In order to increase the accuracy, 6−311+ +G(3df,3pd)[37] and 6−311++G(2d,2p)[38] basis sets have been used for compounds including sulfur and phosphorus, respectively. Calculations have been performed taking into account the experimentally employed solvents by the polarizable continuum model in the integral equation formalism

(IEF-PCM). CYLview software package has been used for visualization purposes.[39]

Similar to ground state calculations, excited state calculations have been carried out by using Gaussian 16 software package. Tamm−Dancoff approximation (TDA) has been used, as this approach avoids unphysically stable triplet states in CT molecules while maintaining a good description of the singlet excited states, hence yielding more accurate and balanced results for ΔE_{ST} calculations.[40,41] The absorption spectra as well as the energies of the lowest lying singlet and triplet excited states have been computed with different functionals (B3LYP,[42−45] BLYP,[42,45,46] PBE0,[43,45,47,48] M06-2X,[42,45,49] CAM-B3LYP,[42,45,50,51] and LC-ωPBE[52−54]) and 6−31 + G(d,p) basis set, and the performances of these functionals have been evaluated with respect to experimental data. Absorption spectra have been modeled, including the effects of vibrational and thermal motion via Wigner distribution sampling of the equilibrium region on the potential energy surface by generating 40 conformations via the Newton-X program[55] on the equilibrium region of the PES.

NTOs and Φ_S indices have been calculated for the S_1 state by using the Gaussian 16 and Nancy_EX program packages,[56] while hole and electron NTOs have been visualized with the Avogadro program package.[57] Φ_S index can be defined as the spatial overlap between attachment and detachment densities. Values closer to 1 indicate the presence of local excitation character, whereas values approaching 0 imply that the CT character is dominant.[56] SOC values between S_1 and T_1, and in some cases between S_1 and T_2, have been calculated using the Amsterdam Density Functional software package by utilizing a DZP basis set.[58]

3. RESULTS AND DISCUSSION

The benzophenone emitters investigated in this study have been grouped according to the type of A moieties used. As depicted in Figure 3, Group 1 emitters are in the form of D-A-D, and they contain benzophenone A cores (in red) bridged with various electron-donating groups. They can be further subdivided into two subgroups: symmetric and asymmetric emitters. Symmetric emitters Px2BP,[12] DMAC-BP,[59] Cz2BP,[12] and CC2BP[12] contain phenoxazine (PXZ), dimethylacridine (DMAC), and carbazole (Cz) donors (in blue), respectively. Asymmetric emitters, A-BP-TA[60] and OPDPO,[61] include D groups such as thianthrene, phenothiazene (PTZ), and diphenylphosphineoxide.

Group 2 emitters have fused D-A ring structures where DBT-BZ-PXZ,[25] DBT-BZ-PTZ,[25] and DBT-BZ-DMAC[24] bear the A unit dibenzothiophene-benzoyl (in red), while CP-BP-PXZ[26] and CP-BP-DMAC[26] have the A unit of phenyl-carbazole-benzoyl (in red). D groups such as PXZ, PTZ, and DMAC have been employed in these emitters as well.

Group 3 emitters have para-substituted structures in which the A unit is anthraquinone.[18] These include D-A-D type emitters a1-a4, in which the D units are diphenylamine (DPA), bis(4-biphenyl)amine, 3,6-di-tert-butylcarbazole, and DMAC, respectively. Similarly, in the D-π-A-π-D structures, b1 and b4, the D groups are DPA and DMAC.

Group 4 emitters have D-A type of structures in which the A unit is xanthone. DMAC, PXZ, and PTZ donors have been used in ACRXTN,[23] 3-PXZ-XO,[20] and PTZ-XT,[62] respectively. In MCz-XT,[21] 1,3,6,8-tetramethylcarbazole is present as the D unit.

Finally, seven non-TADF compounds have been selected from literature in an attempt to elucidate the main structural differences leading to TADF emission (Figure 4). While some of these non-TADF emitters have D-A type structures, including MC2,[63] OPM,[64] and p-Cz,[65] others (ODFRCZ,[66] ODBTCZ,[67] C1,[15] and C2[15]) possess D-A-D type of structures.
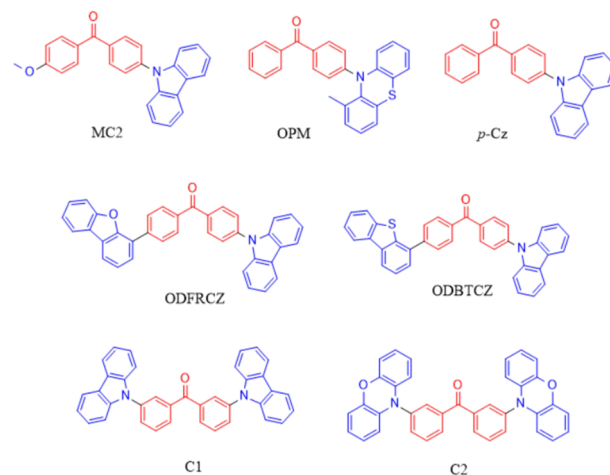

Figure 4. Non-TADF benzophenone emitters.

3.1. Benchmark Calculations and UV−vis Absorption Spectra.
M06-2X/6−31 + G(d,p) and B3LYP-D3/6−31 + G(d,p) methods have been tested for the ground state geometry optimizations of a series of compounds selected from each group. Table S1 depicts the optimized geometries at both levels of theory, and Table S2 includes the D-A torsion angles for the optimized geometries. Tables S1 and S2 suggest that there is no significant change in the geometries optimized at both levels as both functionals yielded similar structures with very close D-A torsion angles. Because the compounds investigated in this study are relatively small in which long-range interactions are not so dominant, we decided to continue with M06-2X/6−31 + G(d,p) for the geometry optimizations because the latter is computationally more affordable.

A series of widely used DFT functionals have been chosen for excited state calculations, BLYP, B3LYP, PBE0, and M06-2X. More specifically, UV−vis absorption spectra have been generated for a group of emitters, and the results have been compared with the available experimental spectra.

The conformational space has been taken into account in the modeling of four compounds (Px2BP, Cz2BP, DBT-BZ-PXZ, and DBT-BZ-DMAC) (Table S1). Their absorption spectra have been obtained as the union of the spectra of all the conformers according to their Boltzmann weights. The merged spectra have then been compared to those obtained from the most stable conformation only. Table S3 clearly demonstrates that weighted conformations exhibit similar photophysical features and spectral shapes as the most stable conformation, the maximum deviation being around 3 nm for B3LYP (DBT-BZ-PXZ), 4 nm for PBE0 (DBT-BZ-PXZ), and 2 nm for M06-2X (Cz2BP). In addition to the UV−vis absorption spectra, different conformations of Cz2BP and CC2BP have very similar ΔE_{ST} values, and the Boltzmann-weighted ΔE_{ST} values of Cz2BP and CC2BP were found to be in good agreement with the experimental findings (Table S4). Thus, henceforth, the most stable conformer will solely be

considered. In Tables S5−S7, the absorption spectra for Group 1 emitters and three emitters from Group 2 have been computed by using BLYP, B3LYP, PBE0, and M06-2X. The results suggest that the spectra obtained with M06-2X exhibit hypsochromic shift as compared to the experimental spectrum.

As opposed to M06-2X, BLYP produced bathochromic shifts and lower ΔE_{ST} values (energies are given in Table S8; histogram charts are depicted in Figures S1 and S2) when compared with the experimental data. This behavior is most probably due to well-known unphysical stabilization of CT states by LDA functionals.[68] In fact, hybrid B3LYP and PBE0 functionals yield the best agreement with experimental spectra and ΔE_{ST}. In order to further confirm this finding, two long-range corrected functionals, CAM-B3LYP and LC-ωPBE, were tested for selected compounds. Table S9 depicts the ΔE_{S1-T1} values (eV) calculated with BLYP, B3LYP, PBE0, CAM-B3LYP, and LC-ωPBE for the S_0 and T_1 optimized geometries of the compounds. Similar to M06-2X, the ΔE_{ST} values calculated with the long-range corrected CAM-B3LYP and LC-ωPBE functionals are significantly higher as compared with experiment and the other functionals. It is also noteworthy that BLYP gave results consistent with the experiment for a few molecules (Px2BP and DMAC-BP). This is probably due to the fact that, due to the relatively small size of the compounds, the CT states are not long-range and hence can be correctly reproduced by hybrid functionals as already observed for instance in some organometallic compounds, hence out-performing medium- or long-range corrected functionals.[69]

In an attempt to take into account the role of excitation on the molecular geometry, the ΔE_{ST} values have been computed from the S_0, S_1, and T_1 geometries with B3LYP, PBE0, and BLYP functionals for a series of compounds, and the results have been reported in Table S10. The results clearly indicate that the ΔE_{ST} values computed from the S_0 and S_1 geometries are usually very similar. This can be explained by the similar molecular structures obtained for S_0 and S_1 geometries (Figure S3), as TADF efficiency relies on the molecular geometry to a great extent. Also, considering the computational cost of S_1 geometry optimizations, for the rest of the calculations, the photophysical properties have been calculated solely with the S_0 and T_1 geometries.

The absorption spectra of all other molecules have hence been calculated with BLYP, B3LYP, and PBE0 functionals (Figures S4−S8). From the results, it can be deduced that compounds with more rigid electron-donating groups such as PXZ, PTZ, and DMAC possess a broadened band (∼350 to 500 nm) appearing after the high intensity local excitation band (∼300 nm), which can be ascribed to the presence of CT states.[70−72] Nevertheless, the reasonably rigid emitters of Group 4 also have blue-shifted absorption spectra, which is most likely due to the less efficient nature of the specific D-A type architecture. Indeed, the presence of a unique D unit might decrease the CT character of the electronic transitions, and coherently reduced T_1-S_1 upconversion efficiency has been previously reported for some D-A type emitters.[73]

Oscillator strengths calculated with B3LYP, PBE0, and BLYP functionals for the transitions from S_0 to S_1, and the reorganization energies between S_0 and S_1 geometries have also been reported in Tables S11 and S12, respectively. While the latter remain low to moderate and are between around 15 and 6 kcal/mol, no systematic behavior between the different classes of molecules can be underlined, thus hampering the use of this parameter to preview TADF efficiency. Low to

moderate geometrical distortion and reorganization energies may also be another reason for the very close ΔE_{ST} values calculated from the S_0 and S_1 geometries. The oscillator strengths were calculated to be near-zero for most of the TADF emitters with very low ΔE_{ST} values and Φ_S indices, for which we assume that the CT characteristics are more pronounced. As is the case in this study, it was previously reported that the oscillator strengths computed at the TDA or full TD-DFT level might be erroneous, especially for the transitions involving CT states.[74]

3.2. D−A Torsion Angles. Several computational TADF descriptors were assessed in order to analyze and investigate the structural and photophysical phenomena related to TADF emissions. One of the most critical TADF descriptors is the torsion angle between the D and A units. The torsion angle must be close to 90° in an ideal TADF emitter because an effective CT configuration can be achieved by spatially separating the hole and electron densities and by breaking the conjugation pattern.[75]

The S_0 and T_1 optimized geometries of all emitters and the conformation energies (M06-2X/6−31 + G(d,p)) are given in Supporting Information (Tables S13−S17). Figure 5 demonstrates the torsion angles measured for all emitters investigated in this study.
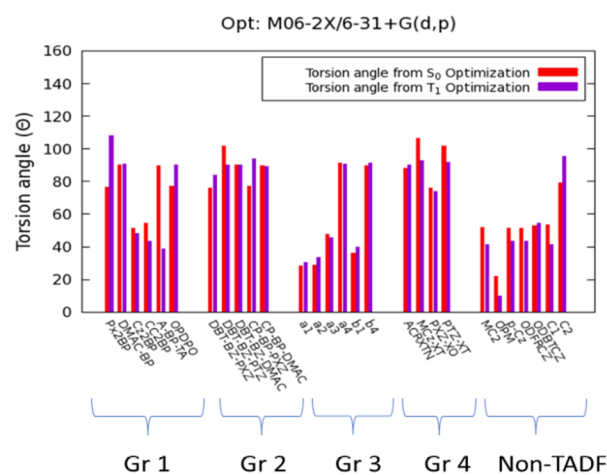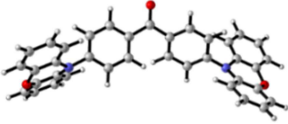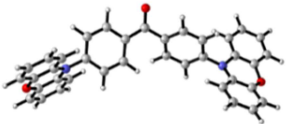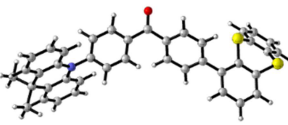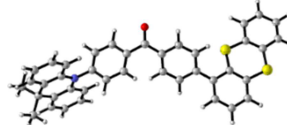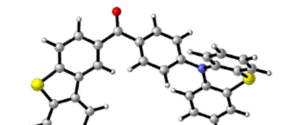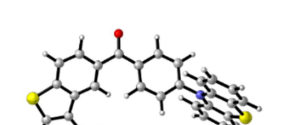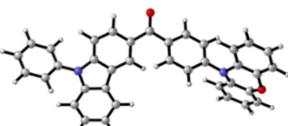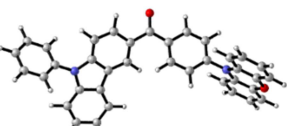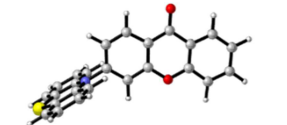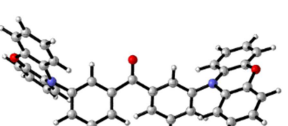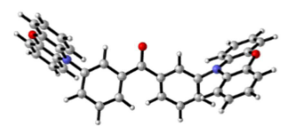
Figure 5. Donor−acceptor torsion angles for the S_0 and T_1 optimized geometries of the investigated emitters shown with stacked histograms (M06-2X/6−31 + G(d,p)).

Because symmetrical emitters have similar torsion angles for each D−A bond, only one of the torsion angles has been shown in Figure 5, while numerical values for torsion angles depicted in Figures S9−S13 are reported in Table S18. For asymmetrical emitters, the torsion angle of the electron-donating unit has been ascribed based on the NTO analysis discussed in the following sections. Similarly, if the electron−hole density is localized on a different electron-donating unit in the T_1 equilibrium geometry, the corresponding torsion angle has been considered for the analysis of the T_1 equilibrium geometries.

It is evident that the emitters containing rigid electron-donating moieties, including DMAC, PXZ, and PTZ, have significantly higher D−A torsion angles. While reasonably high torsion a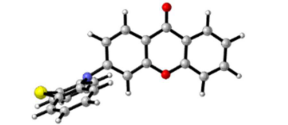ngles have been observed for Group 1, Group 2, and Group 4, Group 3 emitters bear relatively low torsion angles approximately in the range of 30−35°. This feature can be due

Table 1. S_0 and T_1 Geometries of Selected Emitters with Butterfly-Shaped Electron Donors

Compound	S_0 Geometry	T_1 Geometry
Px2BP		
A-BP-TA		
DBT-BZ-PTZ		
CP-BP-PXZ		
PTZ-XT		
C2		

to the presence of less rigid DPA donors whose low steric hindrance may lead to highly planar structure with extended π-conjugation patterns. The highest torsion angles belong to a4 and b4 among Group 3 emitters due to the presence of DMAC electron donors in these groups. Indeed, the additional dimethyl units in the acridine structure impose sterical constraints that restrict the free rotation of the D. Carbazole (Cz)-containing compounds also exhibit low torsion angles, around 55°, which are slightly higher than that for the DPA-bearing compounds. Interestingly, the majority of the non-TADF compounds, where the D unit is Cz, have notably lower torsion angles, along with two compounds from Group 1 emitters (Cz2BP and CC2BP). The torsion angles measured for Group 4 emitters are satisfactorily high and close to 90° regardless of the electron-donating unit. This situation can be attributed to the rigid xanthone skeleton that fixes the D–A torsion angle at a desirable position. This observation is in line with the study of Kreiza et al.[17] Nonetheless, the obtained results suggest that such a descriptor can only provide a partial understanding of TADF efficiency because Group 3 compounds, which are known as TADF emitters, possess very low torsion angles, despite the presence of the rigid anthraquinone A. Hence, a finer analysis of the property and reorganization of the electronic density should be considered to improve TADF efficiency predictions.

While in most cases the torsion angles are similar for both T_1 and S_0 equilibrium geometries, there is a sharp decrease in the torsion angle for T_1 equilibrium geometry in A-BP-TA. Indeed, the hole density in the triplet state is localized on the less rigid electron D thianthrene, causing a rather important planarization of the global structure. This will be better understood in the following section.

3.3. NTOs and Φ_S Indices. NTOs and Φ_S indices have been calculated for all emitters in an attempt to determine the

electron−hole density reorganization. Accordingly, electron and hole NTOs describing electronic density reorganization in the S$_1$ state are shown in Tables S19−S28. Only the NTOs generated from B3LYP/6−31 + G(d,p) densities are given because no remarkable difference has been observed with BLYP and PBE0. Φ$_S$ values describing the spatial overlap between attachment and detachment densities[76] are also reported in Tables S29−S33.

In general, the overlap between electron and hole densities has been observed to be high for compounds bearing low D-A torsion angles. This is expected because low torsion angles cause high degrees of π-delocalization and a corresponding planarization of the molecular core. As a result, compounds bearing Cz and DPA donors, including Cz2BP, CC2BP, a1, a2, a3, b1, and most of the non-TADF compounds, show highly overlapping hole and electron NTOs. Interestingly, in non-TADF emitters ODBTCZ and ODFRCZ, the highly flexible dibenzothiophene and dibenzofuran units did not show electron-donating ability at S$_0$ or T$_1$ equilibrium geometries. Obviously, because high Φ$_S$ indices are indicative of spatially overlapping densities, the corresponding excited states have a more prominent local excitation character. On the other hand, emitters with more rigid D units (DMAC, PXZ, and PTZ) usually have low amounts of overlap between their NTOs, and consequently small Φ$_S$ values, even in the presence of small torsion angles. Hence, even if more computationally expensive, the explicit analysis of the excited state density is much more informative in predicting TADF potential.

It is also noteworthy that the structural reorganization may have an undeniable impact on the amount of CT from the accessible excited states, as in the case of excited state twisting.[77] Indeed, some compounds, particularly those containing butterfly-shaped PXZ, PTZ, or thianthrene units, underwent drastic changes; more specifically, T$_1$ equilibrium geometries exhibited planarization in the butterfly-shaped moieties (Table 1). This, in turn, is related to a change in the shape of the NTOs obtained from the T$_1$ equilibrium geometries. The change in the NTO distribution is indicative of the fact that geometric relaxation leads, for some compounds, such as Px2BP, A-BP-TA, and b1, to the population of a different diabatic state. The most obvious change in the NTO localization pattern is seen in A-BP-TA (Figure 6), where at T$_1$ equilibrium geometry, the hole NTO is localized mostly on the now planar thianthrene unit instead of the rigid DMAC unit. This effect also produces an increase in the Φ$_S$ indices at the T$_1$ equilibrium geometry for Px2BP and its meta-substituted analogue C2 (Tables S19 and S28). The electron NTO localizes only on one of the PXZ units, which becomes planar at T$_1$ equilibrium geometry; this feature is also indicative of a consistent pattern, which is observed in two other similar cases. In the π-bridged anthraquinone-based b1 and b4, similar changes have been observed in the transition from S$_0$ to T$_1$ equilibrium geometry (Table S24). These consist of slight rotations in the bridging phenyl links, which cause disruptions in orthogonality and give rise to an increased electron delocalization. For a better visualization, the hole and electron NTOs and Φ$_S$ indices, calculated at T$_1$ and S$_0$ equilibrium geometries for two TADF and one non-TADF compounds, are shown in Figure 6.

As expected, non-TADF compounds exhibit higher Φ$_S$, which are due to the presence of weaker electron donors like Cz, dibenzofuran, and dibenzothiophene. However, despite the fact that the only noticeable structural difference is related to
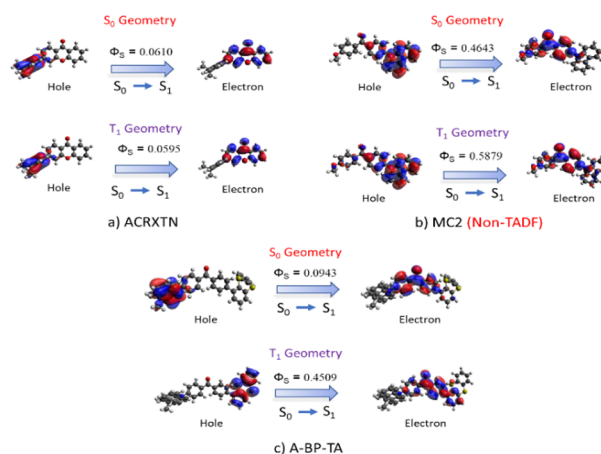

Figure 6. Hole−Electron levels and Φ$_S$ indices calculated with B3LYP/6−31 + G(d,p) for the molecules (a) ACRXTN, (b) MC2, and (c) A-BP-TA.

the position of the PXZ substituents, the meta-substituted non-TADF C2 also exhibits higher Φ$_S$ indices compared to its para-substituted analogue, Px2BP, in line with its classification as a non-TADF compound. Φ$_S$ indices calculated with B3LYP for all compounds are depicted in Figure 7, and the Φ$_S$ indices
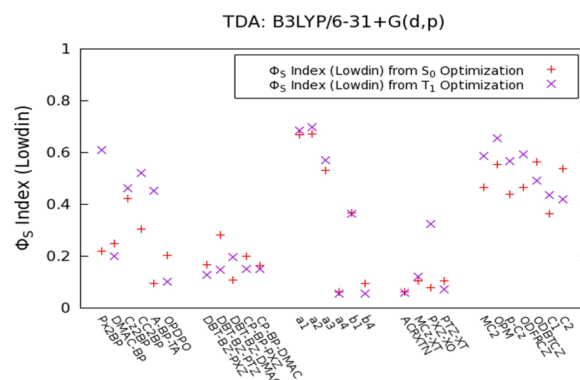

Figure 7. Φ$_S$ indices for the TADF emitters calculated from S$_0$ and T$_1$ geometries with B3LYP/6−31 + G(d,p).

calculated with PBE0 and BLYP are given in Figures S14−S15. TADF behavior is clearly inferred from these values, hence making this descriptor quite promising for the discrimination and prediction of optical properties with TADF potential.

3.4. Singlet−Triplet Energy Gaps (ΔE$_{ST}$).

The energy difference between the first singlet and triplet excited states is an important descriptor for predicting the possibility of TADF emission because the upconversion of T$_1$ to S$_1$ can be achieved only if the energy gap is low enough to be overcome by thermal energy. According to previous studies, ΔE$_{ST}$ values above 0.3 eV usually decrease the likelihood of the RISC process, whereas the upconversion of the triplet becomes more likely if the ΔE$_{ST}$ value is below 0.1 eV.[5]

Even though the RISC process usually takes place from the T$_1$ state, upper lying triplet excited states may also influence the efficiency of RISC if they are in close proximity to T$_1$. Spin-vibronic coupling may cause state mixing between triplet energy levels, giving rise to strongly coupled S$_1$ and T$_1$ states. Therefore, the strong impact of internal conversion on ISC and RISC processes cannot be underestimated.[78] Thus, the energy differences between S$_1$-T$_2$ (ΔE$_{S1-T2}$) states have also been

reported along with the ΔE_{S1-T1} values when the T_2 state lies below S_1 for any given compound. The calculated values together with the experimental findings are reported in Tables S34−S38 and in Figure 8.
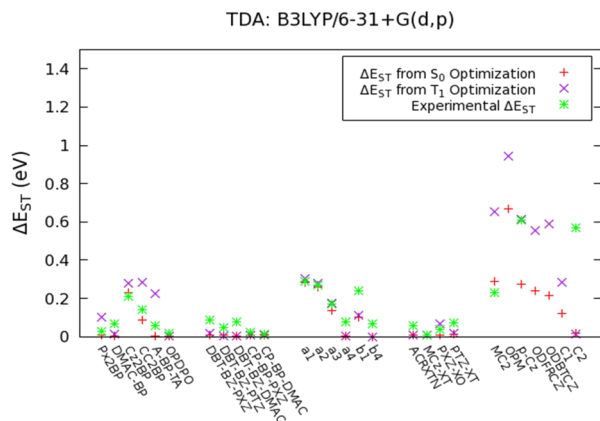

Figure 8. ΔE_{ST} values for TADF emitters calculated from S_0 and T_1 geometries with B3LYP/6−31 + G(d,p). (Experimental ΔE_{ST} values also included).

Figure 8 depicts the ΔE_{S1-T1} values calculated with B3LYP for almost all groups except for Group 3 because ΔE_{S1-T2} values calculated for them are in a better agreement with the experimental findings. It is evident that the lowest ΔE_{ST} values have been obtained from the BLYP calculations, which is consistent with the lowest Φ_S indices computed with this functional. On the other hand, ΔE_{ST} values calculated with B3LYP and PBE0 are closer to the experimental ones. Overall, the calculated ΔE_{ST} values are usually consistent with the experimental observation, especially for the S_0 geometries. The ΔE_{ST} values calculated with PBE0 and BLYP are also given in Figures S16 and S17.

It is noteworthy that ΔE_{ST} values are closely correlated with torsion angles and Φ_S indices because the compounds possessing low torsion angles and high Φ_S indices, such as Cz2BP, CC2BP, most of the Group 3 compounds, and non-TADF compounds, also have relatively higher ΔE_{S1-T2} and in some cases even high ΔE_{S1-T1} values. Freely rotating donors DPA and sterically less hindered donors Cz lead to higher ΔE_{ST} values because of enhanced geometrical relaxation. Despite having DPA donors, b1 has been observed to possess relatively low ΔE_{ST} values, which may have been acquired through the phenyl bridges that lead to a higher spatial separation of electron and hole densities. Also, as expected, emitters with DMAC, PXZ, or PTZ donors have satisfying ΔE_{ST} values usually at both S_0 and T_1 equilibrium geometries due to the induced orthogonality. There is a sharp increase in the ΔE_{ST} values obtained from the T_1 equilibrium geometry of A-BP-TA, where the electron-donating group is the less rigid thianthrene moiety. This is also consistent with the NTO calculations previously mentioned, pointing out the close relationship between ΔE_{ST} and electron−hole separation. This result for A-BP-TA also further proves the reliability of NTO calculations and Φ_S index in elucidating the excited state properties by relating them to the molecular structure.

Almost all of the non-TADF compounds have high ΔE_{ST} values due to higher amounts of density overlap introduced by freely rotating D−A moieties, which planarize to enhance conjugation. However, C2 is an exception as it exhibits notably

lower ΔE_{ST} values in spite of its high Φ_S index and overlapping NTOs. The calculated ΔE_{ST} value is also lower as compared with its experimental ΔE_{ST} value, clearly identifying this compound as an outlier. Still, out of 28 benzophenone derivatives investigated in this study, C2 is the only emitter in which an inverse relationship between ΔE_{ST} values and Φ_S indices was observed, and this can also be resulting from the insufficiency of our methodology in reproducing excited state energies for this compound.

3.5. Spin-Orbit Couplings. The last descriptor analyzed in this study is the SOC. The mixing of the wavefunctions of singlet and triplet energy levels are indeed strongly dictated by SOC.[79] Therefore, by performing SOC calculations, crucial information regarding the feasibility of ISC or RISC processes is obtained. Indeed, SOC matrix elements significantly different from zero are necessary to attain RISC and, hence, TADF emission. However, SOC usually increases with atomic number (Z); thus small organic chromophores are usually less prone to ISC and RISC as compared to heavy-metal containing complexes.[80] Additionally, the coupling of CT states produce negligible SOC values as a consequence of El-Sayed's rule, which highlights the need for local triplet excited states for an effective RISC process.[79] Efficient TADF emitters usually have lower SOC values due to their orthogonal D−A type molecular backbones, where CT character is more pronounced; this unfavorable factor is, however, compensated by small singlet−triplet energy gaps, which are inversely proportional to the (R)ISC probability. Hence, SOC between the S_1 and T_1 states of TADF emitters could also indicate the presence of CT states. Because we are dealing with RISC, calculations were solely performed on equilibrium T_1 geometries. SOC between S_1 and T_2 states have also been computed from the T_1 geometries if the T_2 lies below the S_1 state, in a similar approach adopted for ΔE_{ST} calculations. The calculated SOC values have been reported in Tables S39−S43. For a better comprehension, the SOC values calculated with B3LYP, BLYP, and PBE0 functionals are shown in Figure 9.

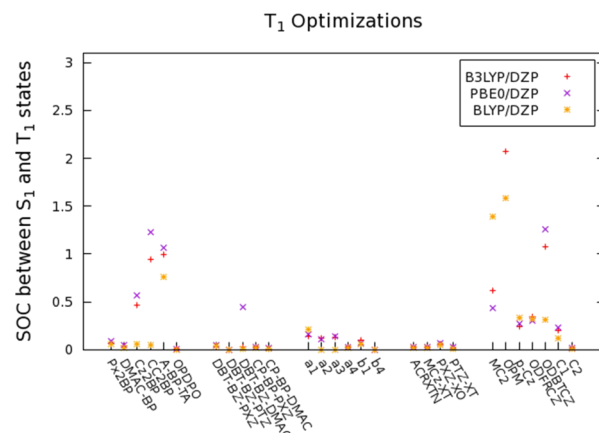**Figure 9.** SOC values for TADF emitters calculated with B3LYP, BLYP, and PBE0 using the T_1 geometries.

The results indicate that the compounds possessing lower ΔE_{ST} values and Φ_S indices, such as most of Group 1 emitters (Px2BP, DMAC-BP, and OPDPO), Group 2 emitters, a4 and b4, and Group 4 emitters, exhibit extremely low SOC values as a result of the higher CT character of their S_1 and T_1 geometries.

Higher SOC values have been obtained for compounds with less steric hindrance, including Cz2BP, CC2BP, most of Group 3 emitters, and all non-TADF emitters, because local excitations become more favorable in these emitters. A-BP-TA also exhibits relatively high SOC values because its hole density becomes localized on the flexible thianthrene unit in its T_1 geometry, reducing the CT character in a similar manner observed in its ΔE_{ST} values and Φ_S index. Additionally, higher SOC constants obtained for S_1-T_2 interactions may indicate that the triplet upconversion might be taking place from the T_2 rather than the T_1 state.

Table 2 summarizes the D−A torsion angle, Φ_S index, ΔE_{ST}, and SOC results of the TADF and non-TADF emitters investigated

Table 2. D−A Torsion Angles (°), Φ_S Indices (Lowdin Charge Population), ΔE_{ST} Values (eV), and SOC Constants for the TADF and Non-TADF Emitters Calculated from the T_1 Geometries (TDA: B3LYP/6−31 + G(d,p))

group	compound	torsion angle	Φ_S index	ΔE_{ST}	SOC
group 1	Px2BP	107.90	0.6097	0.104	0.073
	DMAC-BP	90.91	0.1991	0.013	0.037
	Cz2BP	48.19	0.4603	0.278	0.465
	CC2BP	43.33	0.5206	0.284	0.942
	A-BP-TA	38.90	0.4509	0.225	0.999
	OPDPO	90.06	0.1009	0.004	0.004
group 2	DBT-BZ-PXZ	83.84	0.1279	0.018	0.042
	DBT-BZ-PTZ	90.21	0.1480	0.005	0.002
	DBT-BZ-DMAC	90.11	0.1967	0.004	0.026
	CP-BP-PXZ	93.80	0.1494	0.011	0.026
	CP-BP-DMAC	88.90	0.1514	0.008	0.009
group 3	a1	30.54	0.6839	0.481	0.144
	a2	33.32	0.6992	0.428	0.120
	a3	45.42	0.5689	0.272	0.134
	a4	90.67	0.0546	0.007	0.025
	b1	39.68	0.3627	0.346	0.097
	b4	91.00	0.0544	0.001	0.000
group 4	ACRXTN	90.21	0.0595	0.008	0.025
	MCz-XT	92.89	0.1199	0.011	0.026
	3-PXZ-XO	74.04	0.3243	0.066	0.060
	PTZ-XT	91.49	0.0721	0.018	0.022
non-TADF	MC2	41.45	0.5879	0.651	0.617
	OPM	21.76	0.6566	0.944	2.070
	p-Cz	43.66	0.5675	0.613	0.246
	ODFRCZ	43.69	0.5936	0.553	0.345
	ODBTCZ	52.73	0.4911	0.591	1.078
	C1	41.19	0.4369	0.283	0.202
	C2	95.14	0.4208	0.016	0.015

investigated, showing a consistent behavior for all descriptors studied, pointing toward the successful accuracy of NTOs and Φ_S in inferring the TADF behavior. More importantly, in most cases, the TADF capability may be correctly predicted by calculating the excited state indicators at the Franck−Condon geometry, hence avoiding rather expensive excited state optimizations.

4. CONCLUSIONS

In this study, the photophysical and structural properties of 21 benzophenone-based TADF emitters and 7 benzophenone-based non-TADF emitters have been investigated by using computational descriptors with the aim to elucidate the factors causing RISC. The main descriptors have been identified as the torsion angle between the D and A, NTOs, Φ_S indices, ΔE_{ST} values, and SOC constants.

It was observed that the orthogonality of the molecular backbone is an important factor for achieving a successful RISC process. The compounds adopting a rigid molecular structure where free rotations are more restricted tend to have lower ΔE_{ST} values and Φ_S indices due to increased ICT through well separated electron and hole densities. Conversely, the emitters possessing less rigid and more freely rotating D-A arrangements were observed to have higher ΔE_{ST} values and Φ_S indices due to increased local excitation character induced by high amounts of overlap between the hole and electron and enhanced π-delocalization. Although molecular rigidity relies on both the molecular structures of the D and A, it was shown that the role of D units is more dominant, as freely rotating electron donors such as Cz, DPA, or thianthrene disrupt the orthogonality of the compounds, which leads to, in most cases, lower torsion angles (~30 to 55°). The more rigid electron donors, such as DMAC, PXZ, or PTZ, enhance TADF efficiency through increased orthogonality and electron/hole separation. However, the A rigidity must also be taken into account. The compounds presenting more rigid and planar benzophenone derivatives, such as xanthone, as the A moiety, exhibit satisfying TADF characteristics, regardless of the electron donors. On the contrary, the emitters bearing the benzophenone A, in which the loose phenyl rings have more free rotation, exhibit less satisfying TADF properties. The presence of a π-bridge may also favorably affect the TADF properties owing to the increased spatial separation of D and A units as observed in compounds b1 and b4. Moreover, SOC values were calculated to be lower for the TADF compounds when the presence of highly twisted D-A frameworks induces lower ΔE_{ST} values due to enhanced electron/hole separation.

Excited state calculations were carried out using both S_0 and T_1 geometries because excited state processes, such as RISC, should take place from the T_1 equilibrium geometry. In some cases, a significant geometrical relaxation was observed, in particular for the butterfly-shaped PXZ, PTZ, or thianthrene units, which become planar in T_1 geometry. In these cases, different indicators were obtained for calculations performed at S_0 or T_1 geometries. However, in general, the outcome of the photophysical properties can be correctly inferred by solely considering the Franck−Condon geometry. The benchmark studies revealed that B3LYP and PBE0 can reproduce the excited state energies and UV−vis absorption spectra correctly for almost all emitters, while BLYP yielded satisfying results for several compounds only.

In summary, this study gives a comprehensive outlook on the relationship between molecular structure and photophysical features of a series of benzophenone-based TADF and non-TADF compounds, employing computational tools and several descriptors. It can be concluded that these descriptors, especially the topological Φ_S index, can be safely used to investigate TADF properties of different classes of compounds, as they predict the experimental findings quite accurately.

■ ASSOCIATED CONTENT

ⓢ Supporting Information

The Supporting Information is available free of charge at https://pubs.acs.org/doi/10.1021/acs.jpca.1c08320.

3D representations of the optimized geometries at M06-2X/6−31 + G(d,p) and B3LYP-D3/6−31 + G(d,p) levels, investigation of the conformational effects, benchmark calculations, UV−vis absorption spectra, investigated donor−acceptor torsion angles, hole and electron NTOs, Φ_S indices, low lying singlet−triplet energy gaps, spin-orbit coupling values, and S_0, T_1, and S_1 cartesian coordinates of the most stable conformations optimized at the M06-2X/6−31 + G(d,p) level of theory (PDF)

■ AUTHOR INFORMATION

Corresponding Authors

Viktorya Aviyente − *Department of Chemistry, Bogazici University, 34342 Istanbul, Turkey;* orcid.org/0000-0001-9430-4096; Email: aviye@boun.edu.tr

Saron Catak − *Department of Chemistry, Bogazici University, 34342 Istanbul, Turkey;* orcid.org/0000-0002-4396-8375; Email: saron.catak@boun.edu.tr

Authors

Ekin Esme Bas − *Department of Chemistry, Bogazici University, 34342 Istanbul, Turkey*

Pelin Ulukan − *Department of Chemistry, Bogazici University, 34342 Istanbul, Turkey;* orcid.org/0000-0002-2881-3471

Antonio Monari − *Université de Lorraine and CNRS, F54000 Nancy, France; Université de Paris and CNRS, F75006 Paris, France;* orcid.org/0000-0001-9464-1463

Complete contact information is available at:
https://pubs.acs.org/10.1021/acs.jpca.1c08320

Notes

The authors declare no competing financial interest.

■ ACKNOWLEDGMENTS

■ REFERENCES

(1) Tang, C. W.; VanSlyke, S. A. Organic Electroluminescent Diodes. *Appl. Phys. Lett.* **1987**, *51*, 913−915.

(2) Huang, Y.; Hsiang, E. L.; Deng, M. Y.; Wu, S. T. Mini-LED, Micro-LED and OLED Displays: Present Status and Future Perspectives. *Light-Sci. Appl.* **2020**, *9*, 105.

(3) Tanaka, H.; Shizu, K.; Miyazaki, H.; Adachi, C. Efficient Green Thermally Activated Delayed Fluorescence (TADF) from a Phenoxazine−Triphenyltriazine (PXZ−TRZ) Derivative. *Chem. Commun.* **2012**, *48*, 11392−11394.

(4) Xiao, L.; Chen, Z.; Qu, B.; Luo, J.; Kong, S.; Gong, Q.; Kido, J. Recent Progresses on Materials for Electrophosphorescent Organic Light-Emitting Devices. *Adv. Mater.* **2011**, *23*, 926−952.

(5) Dias, F. B.; Bourdakos, K. N.; Jankus, V.; Moss, K. C.; Kamtekar, K. T.; Bhalla, V.; Santos, J.; Bryce, M. R.; Monkman, A. P. Triplet Harvesting with 100% Efficiency by Way of Thermally Activated Delayed Fluorescence in Charge Transfer OLED Emitters. *Adv. Mater.* **2013**, *25*, 3707−3714.

(6) Zhang, Q.; Li, J.; Shizu, K.; Huang, S.; Hirata, S.; Miyazaki, H.; Adachi, C. Design of Efficient Thermally Activated Delayed Fluorescence Materials for Pure Blue Organic Light Emitting Diodes. *J. Am. Chem. Soc.* **2012**, *134*, 14706−14709.

(7) Endo, A.; Sato, K.; Yoshimura, K.; Kai, T.; Kawada, A.; Miyazaki, H.; Adachi, C. Efficient Up-Conversion of Triplet Excitons into a Singlet State and Its Application for Organic Light Emitting Diodes. *Appl. Phys. Lett.* **2011**, *98*, 2009−2012.

(8) Masui, K.; Nakanotani, H.; Adachi, C. Analysis of Exciton Annihilation in High-Efficiency Sky-Blue Organic Light-Emitting Diodes with Thermally Activated Delayed Fluorescence. *Org. Electron.* **2013**, *14*, 2721−2726.

(9) Uoyama, H.; Goushi, K.; Shizu, K.; Nomura, H.; Adachi, C. Highly Efficient Organic Light-Emitting Diodes from Delayed Fluorescence. *Nature* **2012**, *492*, 234−238.

(10) Reineke, S.; Baldo, M. A. Room Temperature Triplet State Spectroscopy of Organic Semiconductors. *Sci. Rep.* **2014**, *4*, 3797.

(11) Marazzi, M.; Mai, S.; Roca-Sanjuán, D.; Delcey, M. G.; Lindh, R.; González, L.; Monari, A. Benzophenone Ultrafast Triplet Population: Revisiting the Kinetic Model by Surface-Hopping Dynamics. *J. Phys. Chem. Lett.* **2016**, *7*, 622−626.

(12) Lee, S. Y.; Yasuda, T.; Yang, Y. S.; Zhang, Q.; Adachi, C. Luminous Butterflies: Efficient Exciton Harvesting by Benzophenone Derivatives for Full-Color Delayed Fluorescence OLEDs. *Angew. Chem., Int. Ed.* **2014**, *53*, 6402−6406.

(13) Aloïse, S.; Ruckebusch, C.; Blanchet, L.; Réhault, J.; Buntinx, G.; Huvenne, J. P. The Benzophenone S1 (n, π^*)→ T1 (n, π^*) States Intersystem Crossing Reinvestigated by Ultrafast Absorption Spectroscopy and Multivariate Curve Resolution. *J. Phys. Chem A* **2008**, *112*, 224−231.

(14) Huang, B.; Ban, X.; Sun, K.; Ma, Z.; Mei, Y.; Jiang, W.; Lin, B.; Sun, Y. Thermally Activated Delayed Fluorescence Materials Based on Benzophenone Derivative as Emitter for Efficient Solution-Processed Non-Doped Green OLED. *Dyes Pigm.* **2016**, *133*, 380−386.

(15) Keruckiene, R.; Keruckas, J.; Cekaviciute, M.; Volyniuk, D.; Lee, P. H.; Chiu, T. L.; Lee, J. H.; Grazulevicius, J. V. Meta-Substituted Benzophenones as Multifunctional Electroactive Materials for OLEDs. *Dyes Pigm.* **2020**, *174*, No. 108058.

(16) Gan, S.; Zhou, J.; Smith, T. A.; Su, H.; Luo, W.; Hong, Y.; Zhao, Z.; Tang, B. Z. New AIEgens with Delayed Fluorescence for Fluorescence Imaging and Fluorescence Lifetime Imaging of Living Cells. *Mater. Chem. Front.* **2017**, *1*, 2554−2558.

(17) Kreiza, G.; Banevičius, D.; Jovaišaitė, J.; Maleckaitė, K.; Gudeika, D.; Volyniuk, D.; Gražulevičius, J. V.; Juršėnas, S.; Kazlauskas, K. Suppression of Benzophenone-Induced Triplet Quenching for Enhanced TADF Performance. *J. Mater. Chem. C* **2019**, *7*, 11522−11531.

(18) Zhang, Q.; Kuwabara, H.; Potscavage, W. J.; Huang, S.; Hatae, Y.; Shibata, T.; Adachi, C. Anthraquinone-Based Intramolecular Charge-Transfer Compounds: Computational Molecular Design, Thermally Activated Delayed Fluorescence, and Highly Efficient Red Electroluminescence. *J. Am. Chem. Soc.* **2014**, *136*, 18070−18081.

(19) Bin, H.; Ji, Y.; Li, Z.; Zhou, N.; Jiang, W.; Feng, Y.; Lin, B.; Sun, Y. Simple Aggregation−Induced Delayed Fluorescence Materials Based on Anthraquinone Derivatives for Highly Efficient Solution−Processed Red OLEDs. *J. Lumin.* **2017**, *187*, 414−420.

(20) Zhang, Y.; Ma, H.; Wang, S.; Li, Z.; Ye, K.; Zhang, J.; Liu, Y.; Peng, Q.; Wang, Y. Supramolecular Structure-Dependent Thermally-Activated Delayed Fluorescence (TADF) Properties of Organic Polymorphs. *J. Phys. Chem. C* **2016**, *120*, 19759−19767.

(21) Lee, J.; Aizawa, N.; Numata, M.; Adachi, C.; Yasuda, T. Versatile Molecular Functionalization for Inhibiting Concentration Quenching of Thermally Activated Delayed Fluorescence. *Adv. Mater.* **2017**, *29*, No. 1604856.

(22) Aizawa, N.; Tsou, C. J.; Park, I. S.; Yasuda, T. Aggregation-Induced Delayed Fluorescence from Phenothiazine-Containing Donor-Acceptor Molecules for High-Efficiency Non-Doped Organic Light-Emitting Diodes. *Polym. J.* **2017**, *49*, 197−202.

(23) Nakanotani, H.; Higuchi, T.; Furukawa, T.; Masui, K.; Morimoto, K.; Numata, M.; Tanaka, H.; Sagara, Y.; Yasuda, T.; Adachi, C. High-Efficiency Organic Light-Emitting Diodes with Fluorescent Emitters. *Nat. Commun.* **2014**, *5*, 4016.

(24) Guo, J.; Li, X. L.; Nie, H.; Luo, W.; Gan, S.; Hu, S.; Hu, R.; Qin, A.; Zhao, Z.; Su, S. J.; et al. Achieving High-Performance Nondoped OLEDs with Extremely Small Efficiency Roll-Off by Combining Aggregation-Induced Emission and Thermally Activated Delayed Fluorescence. *Adv. Funct. Mater.* **2017**, *27*, No. 1606458.

(25) Guo, J.; Li, X. L.; Nie, H.; Luo, W.; Hu, R.; Qin, A.; Zhao, Z.; Su, S. J.; Tang, B. Z. Robust Luminescent Materials with Prominent Aggregation-Induced Emission and Thermally Activated Delayed Fluorescence for High-Performance Organic Light-Emitting Diodes. *Chem. Mater.* **2017**, *29*, 3623−3631.

(26) Huang, J.; Nie, H.; Zeng, J.; Zhuang, Z.; Gan, S.; Cai, Y.; Guo, J.; Su, S. J.; Zhao, Z.; Tang, B. Z. Highly Efficient Nondoped OLEDs with Negligible Efficiency Roll-Off Fabricated from Aggregation-Induced Delayed Fluorescence Luminogens. *Angew. Chem., Int. Ed.* **2017**, *56*, 12971−12976.

(27) Chen, Z.; Wu, Z.; Ni, F.; Zhong, C.; Zeng, W.; Wei, D.; An, K.; Ma, D.; Yang, C. Emitters with a Pyridine-3,5-Dicarbonitrile Core and Short Delayed Fluorescence Lifetimes of about 1.5 Ms: Orange-Red TADF-Based OLEDs with Very Slow Efficiency Roll-Offs at High Luminance. *J. Mater. Chem. C* **2018**, *6*, 6543−6548.

(28) Olivier, Y.; Sancho-Garcia, J. C.; Muccioli, L.; D'Avino, G.; Beljonne, D. Computational Design of Thermally Activated Delayed Fluorescence Materials: The Challenges Ahead. *J. Phys. Chem. Lett.* **2018**, *9*, 6149−6163.

(29) Mewes, J. M. Modeling TADF in Organic Emitters Requires a Careful Consideration of the Environment and Goingbeyond the Franck-Condon Approximation. *Phys. Chem. Chem. Phys.* **2018**, *20*, 12454−12469.

(30) Kang, S.; Jeon, S. H.; Cho, Y. M.; Kim, Y. J.; Kim, T.; Lee, J. Y. The Key Role of Acceptor Moieties on the Structural and the Electronic Properties of Thermally Activated Delayed Fluorescence Emitters in Excited States: A Computational Study. *Org. Electron.* **2020**, *78*, No. 105595.

(31) Sanz-Rodrigo, J.; Olivier, Y.; Sancho-García, J. C. Computational Studies of Molecular Materials for Unconventional Energy Conversion: The Challenge of Light Emission by Thermally Activated Delayed Fluorescence. *Molecules* **2020**, *25*, 1006.

(32) Zhu, Q.; Guo, X.; Zhang, J. Theoretical Study on Photophysical Properties of a Series of Functional Pyrimidine-Based Organic Light-Emitting Diodes Emitters Presenting Thermally Activated Delayed Fluorescence. *J. Comput. Chem.* **2019**, *40*, 1578−1585.

(33) Tavakoli, M.; Ahmadvand, H.; Alaei, M.; Ranjbari, M. A. Ab-Initio Search for Efficient Red Thermally Activated Delayed Fluorescence Molecules for Organic Light Emitting Diodes. *Spectrochim. Acta A Mol. Biomol. Spectrosc.* **2021**, *246*, No. 118952.

(34) Frisch, G. W.; Schlegel, H. B.; Scuseria, G. E.; Robb, M. A.; Cheeseman, J. R.; Scalmani, G.; Barone, V.; Petersson, G. A.; Nakatsuji, H.; Li, X.; et al. *Gaussian 16, Rev. A.03.*; Gaussian, Inc.: Wallingford, CT, 2016.

(35) Josa, D.; Rodríguez-Otero, J.; Cabaleiro-Lago, E. M.; Rellán-Piñeiro, M. Analysis of the Performance of DFT-D, M05-2X and M06-2X Functionals for Studying $\pi\cdots\pi$ Interactions. *Chem. Phys. Lett.* **2013**, *557*, 170−175.

(36) Darvish Ganji, M.; Hosseini-khah, S. M.; Amini-tabar, Z. Theoretical Insight into Hydrogen Adsorption onto Graphene: A First-principles B3LYP-D3 Study. *Phys. Chem. Chem. Phys.* **2015**, *17*, 2504−2511.

(37) Kolleth, A.; Müller, S.; Lumbroso, A.; Tanriver, G.; Catak, S.; Sulzer-Mossé, S.; De Mesmaeker, A. Access to 3-Aminobenzothio-phenes and 3-Aminothiophenes Fused to 5-Membered Heteroaromatic Rings through 6π-Electrocyclization Reaction of Keteniminium Salts. *Tetrahedron Lett.* **2018**, *59*, 3242−3248.

(38) Zabaradsti, A.; Kakanejadifard, A.; Ghasemian, M. Theoretical Study of Molecular Interactions of Phosphorus Ylide with Hypohalous Acids HOF HOCl and HOBr. *Comput. Theor. Chem.* **2012**, *989*, 1−6.

(39) Legault, C. Y. *CYLview 1.0b*; Université de Sherbrooke, 2009.

(40) Hirata, S.; Head-Gordon, M. Time-Dependent Density Functional Theory within the Tamm-Dancoff Approximation. *Chem. Phys. Lett.* **1999**, *314*, 291−299.

(41) Chantzis, A.; Laurent, A. D.; Adamo, C.; Jacquemin, D. Is the Tamm−Dancoff Approximation Reliable for the Calculation of Absorption and Fluorescence Band Shapes? *J. Chem. Theory Comput.* **2013**, *9*, 4517−4525.

(42) Liang, K.; Zheng, C.; Wang, K.; Liu, W.; Guo, Z.; Li, Y.; Zhang, X. Theoretical Investigation of the Singlet-Triplet Splittings for Carbazole-Based Thermally Activated Delayed Fluorescence Emitters. *Phys. Chem. Chem. Phys.* **2016**, *18*, 26623−26629.

(43) Lu, J.; Zheng, Y.; Zhang, J. Rational Design of Phenoxazine-Based Donor−Acceptor−Donor Thermally Activated Delayed Fluorescent Molecules with High Performance. *Phys. Chem. Phys. Chem.* **2015**, *17*, 20014−20020.

(44) Wang, F.; Hu, J.; Cao, X.; Yang, T.; Tao, Y.; Mei, L.; Zhang, X.; Huang, W. A Low-Cost Phenylbenzoimidazole Containing Electron Transport Material for Efficient Green Phosphorescent and Thermally Activated Delayed Fluorescent OLEDs. *J. Mater. Chem. C* **2015**, *3*, 5533−5540.

(45) Cardeynaels, T.; Paredis, S.; Deckers, J.; Brebels, S.; Vanderzande, D.; Maes, W.; Champagne, B. Finding the Optimal Exchange−Correlation Functional to Describe the Excited State Properties of Push−Pull Organic Dyes Designed for Thermally Activated Delayed Fluorescence. *Phys. Chem. Phys. Chem.* **2020**, *22*, 16387−16399.

(46) Bhattacharjee, I.; Acharya, N.; Ray, D. Thermally Activated Delayed Fluorescence and Room-Temperature Phosphorescence in Naphthyl Appended Carbazole−Quinoline Conjugates, and Their Mechanical Regulation. *Chem. Commun.* **2019**, *55*, 1899−1902.

(47) Sagara, Y.; Shizu, K.; Tanaka, H.; Miyazaki, H.; Goushi, K.; Kaji, H.; Adachi, C. Highly Efficient Thermally Activated Delayed Fluorescence Emitters with a Small Singlet−Triplet Energy Gap and Large Oscillator Strength. *Chem. Lett.* **2015**, *44*, 360−362.

(48) Alipour, M.; Karimi, N. Dissecting the Accountability of Parameterized and Parameter-Free Single-Hybrid and Double-Hybrid Functionals for Photophysical Properties of TADF-Based OLEDs. *J. Chem. Phys.* **2017**, *146*, 234304.

(49) Shizu, K.; Uejima, M.; Nomura, H.; Sato, T.; Tanaka, K.; Kaji, H.; Adachi, C. Enhanced Electroluminescence from a Thermally Activated Delayed-Fluorescence Emitter by Suppressing Nonradiative Decay. *Phys. Rev. Applied* **2015**, *3*, No. 014001.

(50) Tanaka, H.; Shizu, K.; Lee, J.; Adachi, C. Effect of Atom Substitution in Chalcogenodiazole-Containing Thermally Activated Delayed Fluorescence Emitters on Radiationless Transition. *J. Phys. Chem. C* **2015**, *119*, 2948−2955.

(51) Woo, S. J.; Kim, J. J. TD-DFT and Experimental Methods for Unraveling the Energy Distribution of Charge-Transfer Triplet/Singlet States of a TADF Molecule in a Frozen Matrix. *J. Phys. Chem. A* **2021**, *125*, 1234−1242.

(52) Kim, H. S.; Lee, J. Y.; Shin, S.; Jeong, W.; Lee, S. H.; Kim, S.; Lee, J.; Suh, M. J.; Yoo, S. Enhancement of Reverse Intersystem Crossing in Charge-Transfer Molecule through Internal Heavy Atom Effect. *Adv. Funct. Mater.* **2021**, *31*, No. 2104646.

(53) Fan, J.; Cai, L.; Lin, L.; Wang, C. -K. Excited State Dynamics for Hybridized Local and Charge Transfer State Fluorescent Emitters with Aggregation-Induced Emission in the Solid Phase: A QM/MM Study. *Phys. Chem. Chem. Phys.* **2017**, *19*, 29872−29879.

(54) Kim, D. H.; Inada, K.; Zhao, L.; Komino, T.; Matsumoto, N.; Ribierre, J. C.; Adachi, C. Organic Light Emitting Diodes with Horizontally Oriented Thermally Activated Delayed Fluorescence Emitters. *J. Mater. Chem. C* **2017**, *5*, 1216−1223.

(55) Barbatti, M.; Ruckenbauer, M.; Plasser, F.; Pittner, J.; Granucci, G.; Persico, M.; Lischka, H. Newton-X: A Surface-Hopping Program for Nonadiabatic Molecular Dynamics. *WIREs. Comput. Mol. Sci.* **2014**, *4*, 26−33.

(56) Etienne, T.; Assfeld, X.; Monari, A. New Insight into the Topology of Excited States through Detachment/Attachment Density Matrices-Based Centroids of Charge. *J. Chem. Theory Comput.* **2014**, *10*, 3906−3914.

(57) Hanwell, M. D.; Curtis, D. E.; Lonie, D. C.; Vandermeersch, T.; Zurek, E.; Hutchison, G. R. Avogadro: An Advanced Semantic Chemical Editor, Visualization, and Analysis Platform. *Aust. J. Chem.* **2012**, *4*, 1−17.

(58) te Velde, G.; Bickelhaupt, F. M.; Baerends, E. J.; Fonseca Guerra, C.; van Gisbergen, S. J. A.; Snijders, J. G.; Ziegler, T. Chemistry with ADF. *J. Comput. Chem.* **2001**, *22*, 931−967.

(59) Zhang, Q.; Tsang, D.; Kuwabara, H.; Hatae, Y.; Li, B.; Takahashi, T.; Lee, S. Y.; Yasuda, T.; Adachi, C. Nearly 100% Internal Quantum Efficiency in Undoped Electroluminescent Devices Employing Pure Organic Emitters. *Adv. Mater.* **2015**, *27*, 2096−2100.

(60) Tomkeviciene, A.; Matulaitis, T.; Guzauskas, M.; Andruleviciene, V.; Volyniuk, D.; Grazulevicius, J. V. Thianthrene and Acridan-Substituted Benzophenone or Diphenylsulfone: Effect of Triplet Harvesting via TADF and Phosphorescence on Efficiency of All-Organic OLEDS. *Org. Electron.* **2019**, *70*, 227−239.

(61) Chen, X.; Yang, Z.; Xie, Z.; Zhao, J.; Yang, Z.; Zhang, Y.; Aldred, M. P.; Chi, Z. An Efficient Yellow Thermally Activated Delayed Fluorescence Emitter with Universal Applications in Both Doped and Non-Doped Organic Light-Emitting Diodes. *Mater. Chem. Front.* **2018**, *2*, 1017−1023.

(62) Lee, I. H.; Song, W.; Lee, J. Y. Aggregation-Induced Emission Type Thermally Activated Delayed Fluorescent Materials for High Efficiency in Non-Doped Organic Light-Emitting Diodes. *Org. Electron.* **2016**, *29*, 22−26.

(63) Wei, Q.; Kleine, P.; Karpov, Y.; Qiu, X.; Komber, H.; Sahre, K.; Kiriy, A.; Lygaitis, R.; Lenk, S.; Reineke, S.; Voit, B. Conjugation-Induced Thermally Activated Delayed Fluorescence (TADF): From Conventional Non-TADF Units to TADF-Active Polymers. *Adv. Funct. Mater.* **2017**, *27*, No. 1605051.

(64) Chen, C.; Huang, R.; Batsanov, A. S.; Pander, P.; Hsu, Y.-T.; Chi, Z.; Dias, F. B.; Bryce, M. R. Intramolecular Charge Transfer Controls Switching Between Room Temperature Phosphorescence and Thermally Activated Delayed Fluorescence. *Angew. Chem. Int. Ed.* **2018**, *130*, 16645−16649.

(65) Mao, Z.; Yang, Z.; Xu, C.; Xie, Z.; Jiang, L.; Gu, F. L.; Zhao, J.; Zhang, Y.; Aldred, M. P.; Chi, Z. Two-Photon-Excited Ultralong Organic Room Temperature Phosphorescence by Dual-Channel Triplet Harvesting. *Chem. Sci.* **2019**, *10*, 7352−7357.

(66) Huang, L.; Liu, L.; Li, X.; Hu, H.; Chen, M.; Yang, Q.; Ma, Z.; Jia, X. Crystal-State Photochromism and Dual-Mode Mechanochromism of an Organic Molecule with Fluorescence, Room-Temperature Phosphorescence, and Delayed Fluorescence. *Angew. Chem. Int. Ed.* **2019**, *131*, 16597−16602.

(67) Huang, L.; Liu, J.; Liu, L.; Yang, Q.; Ma, Z.; Jia, X. A D-A-D' Type Organic Molecule with Persistent Phosphorescence Exhibiting Dual-Mode Mechanochromism. *Dyes Pigm.* **2020**, *173*, No. 107963.

(68) Wanko, M.; García-Risueño, P.; Rubio, A. Excited States of the Green Fluorescent Protein Chromophore: Performance of Ab Initio and Semi-Empirical Methods. *Phys. Status Solidi B Basic Res.* **2012**, *249*, 392−400.

(69) Very, T.; Despax, S.; Hébraud, P.; Monari, A.; Assfeld, X. Spectral Properties of Polypyridyl Ruthenium Complexes Intercalated in DNA: Theoretical Insights into the Surrounding Effects of [Ru(Dppz)(Bpy) 2]2+. *Phys. Chem. Chem. Phys.* **2012**, *14*, 12496−12504.

(70) Laguitton-Pasquier, H.; Pansu, R.; Chauvet, J.-P.; Collet, A.; Faure, J.; Lapouyade, R. The Charge Transfer State of Excited Bianthryl and a Derivative: Solvatochromism, Emission CT Spectra Broadening in Homogeneous Solvents. *Chem. Phys.* **1996**, *212*, 437−455.

(71) Banerjee, S.; Both, A. K.; Sarkar, M. Probing the Aggregation and Signaling Behavior of Some Twisted 9,9′-Bianthryl Derivatives: Observation of Aggregation-Induced Blue-Shifted Emission. *ACS Omega* **2018**, *3*, 15709−15724.

(72) Numata, M.; Yasuda, T.; Adachi, C. High Efficiency Pure Blue Thermally Activated Delayed Fluorescence Molecules Having 10H-Phenoxaborin and Acridan Units. *Chem. Commun.* **2015**, *51*, 9443−9446.

(73) Chen, X. K.; Zhang, S. F.; Fan, J. X.; Ren, A. M. Nature of Highly Efficient Thermally Activated Delayed Fluorescence in Organic Light-Emitting Diode Emitters: Nonadiabatic Effect between Excited States. *J. Phys. Chem. C* **2015**, *119*, 9728−9733.

(74) Olivier, Y.; Moral, M.; Muccioli, L.; Sancho-García, J. C. Dynamic Nature of Excited States of Donor−Acceptor TADF Materials for Oleds: How Theory Can Reveal Structure−Property Relationships. *J. Mater. Chem. C* **2017**, *5*, 5718−5729.

(75) Meng, G.; Chen, X.; Wang, X.; Wang, N.; Peng, T.; Wang, S. Isomeric Bright Sky-Blue TADF Emitters Based on Bisacridine Decorated DBNA: Impact of Donor Locations on Luminescent and Electroluminescent Properties. *Adv. Opt. Mater.* **2019**, *7*, No. 1900130.

(76) Etienne, T.; Gattuso, H.; Michaux, C.; Monari, A.; Assfeld, X.; Perpète, E. A. Fluorene-Imidazole Dyes Excited States from First-Principles Calculations—Topological Insights. *Theor. Chem. Acc.* **2016**, *135*, No. 1900130.

(77) Gulbinas, V.; Kodis, G.; Jursenas, S.; Valkunas, L.; Gruodis, A.; Mialocq, J. C.; Pommeret, S.; Gustavsson, T. Charge Transfer Induced Excited State Twisting of N,N-Dimethylaminobenzylidene-1,3-Indandione in Solution. *J. Phys. Chem. A* **1999**, *103*, 3969−3980.

(78) Huang, R.; Avó, J.; Northey, T.; Chaning-Pearce, E.; Dos Santos, P. L.; Ward, J. S.; Data, P.; Etherington, M. K.; Fox, M. A.; Penfold, T. J.; Berberan-Santos, M. N.; Lima, J. C.; et al. The Contributions of Molecular Vibrations and Higher Triplet Levels to the Intersystem Crossing Mechanism in Metal-Free Organic Emitters. *J. Mater. Chem. C* **2017**, *5*, 6269−6280.

(79) Huang, T.; Jiang, W.; Duan, L. Recent Progress in Solution Processable TADF Materials for Organic Light-Emitting Diodes. *J. Mater. Chem. C* **2018**, *6*, 5577−5596.

(80) Marian, C. M. Spin-Orbit Coupling and Intersystem Crossing in Molecules. *WIREs. Comput. Mol. Sci* **2012**, *2*, 187−203.